

See discussions, stats, and author profiles for this publication at: <https://www.researchgate.net/publication/38081454>

Liquid-Crystalline Nematic Phase in Aqueous Suspensions of a Disk-Shaped Natural Beidellite Clay

ARTICLE *in* THE JOURNAL OF PHYSICAL CHEMISTRY B · NOVEMBER 2009

Impact Factor: 3.3 · DOI: 10.1021/jp908326y · Source: PubMed

CITATIONS

57

READS

81

11 AUTHORS, INCLUDING:



Krassimira Antonova
Bulgarian Academy of Sciences

40 PUBLICATIONS 285 CITATIONS

[SEE PROFILE](#)



Patrick Davidson
Université Paris-Sud 11

176 PUBLICATIONS 4,492 CITATIONS

[SEE PROFILE](#)



Marianne Impéror-Clerc
Université Paris-Sud 11

83 PUBLICATIONS 1,951 CITATIONS

[SEE PROFILE](#)



Florian Meneau
Centro Nacional de Pesquisa em Energia e ...

71 PUBLICATIONS 993 CITATIONS

[SEE PROFILE](#)

Liquid-Crystalline Nematic Phase in Aqueous Suspensions of a Disk-Shaped Natural Beidellite Clay

E. Paineau,^{*,†} K. Antonova,[‡] C. Baravian,[§] I. Bihannic,[†] P. Davidson,^{||} I. Dozov,[‡] M. Impérator-Clerc,^{||} P. Levitz,[⊥] A. Madsen,[#] F. Meneau,[▽] and L. J. Michot^{*,†}

Laboratoire Environnement et Minéralurgie, Nancy University CNRS-INPL UMR 7569, BP40 54501 Vandœuvre Cedex France, Institute of Solid State Physics, Bulgarian Academy of Sciences, Boulevard Tzarigradsko Chaussee 72, Sofia, 1784, Bulgaria, Laboratoire d'Energétique et de Mécanique Théorique et Appliquée, Nancy University UMR 7563 CNRS-INPL-UHP, 2, Avenue de la Forêt de Haye, BP160 54504 Vandœuvre Cedex, France, Laboratoire de Physique des Solides, UMR 8502 CNRS-Université Paris-Sud Bât 510 91405 Orsay Cedex France, Laboratoire de Physique de la Matière Condensée, UMR 7643 CNRS-Polytechnique Ecole Polytechnique 91128 Palaiseau Cedex, France, European Synchrotron Radiation Facility, BP220, 38043, Grenoble, France, and Synchrotron SOLEIL, BP48, 91192, Gif-sur-Yvette Cedex France

Received: August 28, 2009; Revised Manuscript Received: October 21, 2009

After size-selection and osmotic pressure measurements at fixed ionic strength, the behavior of aqueous colloidal suspensions of anisotropic disklike beidellite clay particles has been investigated by combining optical observations under polarized light, rheological, and small angle X-ray scattering (SAXS) experiments. The obtained phase diagrams (volume fraction/ionic strength) reveal, for ionic strength below 10^{-3} M/L, a first-order isotropic/nematic (I/N) phase transition before gel formation at low volume fractions, typically around 0.5%. This I/N transition line displays a positive slope for increasing ionic strength and shifts toward lower volume fraction with increasing particle size, confirming that the system is controlled by repulsive interactions. The swelling laws, derived from the interparticle distances obtained by SAXS, display a transition from isotropic swelling at low volume fractions to lamellar swelling at higher volume fractions. The liquid-crystal properties have then been investigated in detail. Highly aligned nematic samples can be obtained in three different ways, by applying a magnetic field, an ac electric field, and by spontaneous homeotropic anchoring on surfaces. The birefringence of the fluid nematic phase is negative with typical values around 5×10^{-4} at a volume fraction of about 0.6%. High nematic order parameters have been obtained as expected for well-aligned samples. The nematic director is aligned parallel to the magnetic field and perpendicular to the electric field.

Introduction

Suspensions of anisotropic colloidal particles can exhibit phase transitions due to spontaneous self-assembling processes that lead to various liquid-crystalline phases.¹ Nematic ordering in suspensions of rodlike particles was probably first reported by Zocher for V_2O_5 suspensions.² As theoretically rationalized by Onsager, an isotropic (I) to nematic (N) phase transition can occur for rodlike particles as the result of a competition between orientational entropy and the packing entropy governed by excluded-volume interactions.³ Liquid-crystalline ordering has indeed been observed in numerous colloidal suspensions of rodlike particles and, among these, mineral ones have lately been the focus of a renewed interest.^{4–7} Actually, Onsager's ideas also apply to suspensions of platelike particles, as was later confirmed by computer simulations,⁸ and liquid-crystalline order has also been recently reported for suspensions of disklike crystallites, like gibbsite, a system synthesized and investigated

in-depth by scientists of the Van't Hoff Laboratory in Utrecht^{9–13} or synthetic monodisperse nickel hydroxide colloids that also leads to columnar phases^{14,15}

In this context, the case of colloidal aqueous suspensions of swelling clays is less clear. Swelling clay minerals are composed of an octahedral sheet (Al, Fe, Mg) sandwiched between two opposite tetrahedral sheets (Si, Al, Fe). This 2/1 structure carries a negative charge due to isomorphic substitutions that are compensated by exchangeable cations present in the interlayer space. These materials are highly anisotropic with typical aspect ratios between 20 and 1000 and thicknesses below a nanometer. When fully exfoliated in water, they may provide suspensions likely to display liquid-crystalline order. Such a phenomenon was indeed reported by Langmuir for suspensions of California hectorite.¹⁶ However, as he mentioned in his original paper, this observation was not reproducible. Later studies performed with either laponite, a synthetic clay,^{17–20} or natural swelling clays²¹ have not allowed the detection of a true thermodynamic liquid-crystalline ordering because of the existence at low volume fractions of a sol/gel transition. Nevertheless, nematic textures have been reported for gel samples^{21–23} while scattering techniques^{24–30} or X-ray microscopy studies³¹ have revealed nematic-like orientational order in the gel phase.

Recently, Michot et al. studied the phase behavior of aqueous suspensions of a natural clay mineral, namely nontronite, a Fe-

* To whom correspondence should be addressed. E-mail: laurent.michot@ensg.inpl-nancy.fr.

[†] Nancy University CNRS-INPL UMR 7569.

[‡] Bulgarian Academy of Sciences.

[§] Nancy University UMR 7563 CNRS-INPL-UHP.

^{||} UMR 8502 CNRS-Université Paris-Sud.

[⊥] UMR 7643 CNRS-Polytechnique.

[#] European Synchrotron Radiation Facility.

[▽] Synchrotron SOLEIL.

rich beidellite, member of the montmorillonite group.³² These suspensions were shown to display a “true” isotropic/nematic phase transition, the position of which depends on average platelet size.³³ Furthermore, rheological and small-angle X-ray scattering measurements of the different phases confirmed the repulsive nature of this system at low ionic strength ($\leq 10^{-3}$ M/L).^{33,34} Similar features were obtained lately using another type of nontronite clay with a higher layer charge.³⁵ However, the platelike particles of both nontronite systems are actually lath-shaped, which can somehow complicate the interpretation of their behavior due to the existence of a large in-plane shape anisotropy.

In this work, we report the phase behavior of natural beidellite suspensions (SBId-1) and their spontaneous nematic ordering. In contrast with nontronite, beidellite platelets are subhedral lamellae with a disklike morphology. After size-selection, a wide concentration range of aqueous beidellite suspensions at various ionic strengths has been analyzed by combining observations in polarized light and rheological experiments in order to determine the phase diagrams and to assess the influence of particle size and ionic strength. Then, small-angle X-ray scattering experiments have been performed throughout the whole phase diagrams in order to study the organization and orientation of the particles in the different phases. Finally, nematic beidellite suspensions have been completely aligned by confinement in flat glass capillaries and by applying magnetic and/or electric fields. This last point nicely illustrates the opportunities afforded by liquid-crystalline properties in order to improve the processing of such materials.

Materials and Methods

Beidellite is a natural dioctahedral swelling clay mineral with a charge deficit located in the tetrahedral sheet, resulting from the substitution of Si by Al. This mineral then represents the Al-rich end-member of the montmorillonite–beidellite–nontronite isomorphous series.³⁶ Natural samples of beidellite SBId-1 were purchased from the Source Clays Minerals Repository of the Clay Mineral Society at Purdue University. Rock samples were originally extracted from veins and lenses in rhyolite alteration beds close to the surface into the first bench of Glen Silver pit from the DeLamar mine in Southwest Idaho.³⁷ Clay suspensions were purified following the procedure established previously for nontronites.^{30,32} After grinding the raw sample, a $40 \text{ g} \cdot \text{L}^{-1}$ clay suspension was exchanged three times in 1 M NaCl solution during 24 h. Excess chloride was then removed by dialyzing the suspension against Milli-Q water until the conductivity was below $5 \mu\text{S}/\text{m}$. After recovery from the dialysis tubes, the suspension was then transferred into Imhoff cones and was left to sediment during 24 h. The supernatant was then siphoned off as the bottom of the cone contains miscellaneous impurities (mainly sand-size quartz, feldspar, and iron and titanium oxyhydroxydes) that were discarded. The structural formula of the purified beidellite was defined by Post et al. as $(\text{Si}_{7.27}\text{Al}_{0.73})(\text{Al}_{3.77}\text{Fe}^{3+}_{0.11}\text{Mg}_{0.21})\text{O}_{20}(\text{OH})_4\text{Na}_{0.67}$.³⁷ By using the unit-cell parameters, the density of beidellite can be estimated to be around $2.6 \text{ g}/\text{cm}^3$. To reduce polydispersity, size fractionation procedures were then applied. The stock suspension was first centrifuged at 7000g during 90 min. The sediment was collected, rediluted in Milli-Q water, and will be referred to as “size 1” hereafter. The same procedure was then applied after centrifugations at 17000 and 35000g thus yielding “size 2” and “size 3” fractions. For each size, the mineralogical purity was checked by X-ray diffraction and infrared spectrometry while the cationic exchange capacity (CEC) was determined by

exchange with cobalthexamine.³⁸ Its value is independent of particle size and is equal to around $85\text{meq}/100 \text{ g}$ that corresponds to a nominal charge $C \approx -0.1 \text{ C}/\text{m}^2$ by taking into account unit cell dimensions.

The size of individual particles was determined by transmission electron microscopy (TEM) using a CM12 Philips microscope operating at 80 keV. One drop of a dilute beidellite suspension ($\approx 20 \text{ mg}/\text{L}$) was deposited and air-dried on a carbon-coated copper grid before observation. For each size, the mean diameter $\langle D \rangle$ and its polydispersity σ_D , defined as the relative standard deviation:

$$\sigma_D = \frac{\sqrt{\langle D^2 \rangle - \langle D \rangle^2}}{\langle D \rangle} \quad (1)$$

were determined from the analysis of around 150 particles.

To scan the whole (volume fraction/ionic strength) phase diagram, homogeneous suspensions were prepared by osmotic stress³⁹ using dialysis tubes (Visking) with a molecular weight cutoff of 14000 Da. Beforehand, the membranes were rinsed twice with a 10^{-3} M sodium chloride solution to remove impurities, washed twice more in Milli-Q water, and then stored at the ionic strength of the experiment during one night. Simultaneously, solutions of different osmotic pressures were prepared by dilution of PEG 20000 (Roth) in sodium chloride solutions. To fulfill the conditions of an osmotic stress, in the case of solutions with low osmotic pressures ($\Pi_{\text{osm}} \leq 1300 \text{ Pa}$), membranes were filled with 60 cm^3 of clay suspension and placed in 250 cm^3 of PEG solutions. For higher pressures, either 90 or 120 cm^3 of clay suspensions were respectively placed into 500 or 1000 cm^3 of PEG solutions. PEG solutions were renewed after two weeks, and the experiment was stopped after one month as it was shown previously for latexes,⁴⁰ laponite,^{18,41} and nontronite,³³ that such a time was ensuring osmotic equilibrium. At the end of the experiment, the beidellite suspensions were recovered and their mass concentrations were determined by weight loss upon drying, taking into account the relative humidity according to the water adsorption isotherm of Na-saponite.⁴²

The birefringence of the samples was assessed by optical observations following two different procedures. For naked-eye observations between crossed polarizers, beidellite samples were transferred in 2 cm^3 glass vials with a diameter of 5 mm. This method can only be applied in the case of moderately concentrated suspensions because of multiple scattering affecting more concentrated systems. In parallel, samples were introduced into flat capillaries (VitroCom, $0.2 \times 2 \text{ mm}$) and stored vertically after flame-sealing. The phase separation was then observed using a Nikon optical microscope equipped with crossed polarisers.

Rheological measurements were performed on an Aspect Rheometer 2000 (TA Instruments) with a small cone and plate geometry (2 cm, 0.30° , $14 \mu\text{m}$ truncation). The elastic G' and viscous G'' moduli were measured in oscillatory mode using frequencies between 0.02 and 10 Hz. The stress used in the oscillatory measurements was adjusted in order to remain in the linear regime.

Small angle X-ray scattering (SAXS) experiments have been performed to determine the organization of beidellite platelets in the suspensions both at synchrotron radiation facilities and with an in-house setup. The samples were held in cylindrical glass capillaries (diameter = 1 mm, GLAS, Schönwalde bei Berlin, Germany) of 1 mm diameter that were flame-sealed.

SAXS measurements were carried out on beamlines BW4 at Hasylab (Hamburg, Germany), D2AM and ID10A at ESRF (Grenoble, France) at a fixed wavelength of 0.138, 0.110, and 0.155 nm, respectively, and using a sample to detector distance of 13, 1.60, and 2.15 m, respectively. Two-dimensional (2D) scattering patterns were collected either on a CCD camera or on a “Medipix” pixelated 2D detector. Additional SAXS measurements were also performed at the SWING beamline of SOLEIL (Orsay, France) for samples previously aligned in a 8 T magnetic field delivered by a superconducting magnet. The wavelength was fixed at 0.112 nm and the 2D scattering patterns were collected on an AVIEX CCD camera.

The in-house SAXS setup was already described.⁴³ The X-ray beam is produced by a copper-rotating anode generator (Rigaku RU-200BEH), monochromatized ($\lambda = 0.154$ nm) by an Osmic point-focusing optics and then collimated by three successive pairs of slits. This setup was used to investigate samples aligned by applying an electric field in situ.

In all cases, angular integration of the scattering patterns gave the dependence of the scattered intensity versus scattering vector modulus q ($q = 4\pi \sin \theta/\lambda$, where 2θ is the scattering angle and λ is the wavelength). For anisotropic patterns, the angular integration was reduced around the direction of maximum intensity. The alignment of suspensions that showed anisotropic patterns was assessed by extracting angular profiles of the scattered intensity at constant q .

Samples of beidellite suspensions in the fluid nematic phase, held in either cylindrical or flat glass capillaries, could be aligned in a few hours in the ~8 T magnetic field delivered by a superconducting magnet. They were then removed from the field and studied both by polarized light microscopy and by SAXS.

The study of the alignment of beidellite suspensions under electric field used an experimental setup specially adapted to avoid sample degradation by electrolysis and to minimize the measurement artifacts due to charge migration, water evaporation, etc. The samples were filled and sealed in glass capillaries, either cylindrical for the SAXS measurements, or flat (optical path = 100, 200, or 300 μm) for optical observations. The electric field, parallel to the capillary long axis, is applied using external electrodes, two rings of aluminum foil fixed at the capillary wall and $L = 1$ mm apart. High frequency ($f = 10\text{kHz}$ to 1 MHz) sinusoidal ac voltage with amplitude U up to 200 V is applied to the electrodes using a function generator and fast amplifier (Krohn-Hite 7602M). Numerical calculations of the electric field \mathbf{E} penetrating in the sample, to be presented in detail in a forthcoming paper, show that the field is rather uniform in the interelectrode area (less than 5% variation) with effective rms value given by

$$\mathbf{E} = \frac{1}{\sqrt{2}} C_d C_s(f) \frac{U}{L} \quad (2)$$

Here, $C_d \sim 0.5$ is a correction for the dielectric losses that depends on the sample geometry and the dielectric constants of the suspension ($\epsilon \sim 80$) and of the glass wall ($\epsilon_g \sim 3$), and $C_s(f)$ takes into account the frequency-dependent screening of the field due to the charge accumulation on the suspension/wall interface. In fact, up to the charge relaxation frequency $f_c = \sigma/(2\pi\epsilon_0\epsilon)$, σ being the sample conductivity, the potential drop is mainly located in the thin layer of ions accumulated at the glass wall which serves in our experiment as a blocking layer, preventing charge exchange with the electrodes. However, for $f \gg f_c$ the charges cannot follow the rapidly varying field and the screening losses become negligible, $C_s(f) \sim 1$. The electric

field experiments reported here are performed in this regime, taking into account the experimentally measured value $f_c = 50$ kHz to 300 kHz, depending on the ionic strength of the suspension. Optical observations of the texture changes under electric field are carried out with a polarizing microscope (Olympus BX-51) equipped with a Canon Camedia C-3030 CCD camera and with a Berek compensator for the birefringence measurements ($\Delta n = n_e - n_o$). The electric-field setup could also be positioned on the in-house SAXS setup for in situ scattering experiments.

Results and Discussion

1. Phase Diagrams. Particle Characterization. Figure 1 presents beidellite samples observed by transmission electron microscopy. The clay platelets exhibit irregular crystalline outlines classified as a subhedral shape⁴⁴ similar to what is observed for montmorillonite.^{21,45} Because of the irregular shape of the particles, the diameter chosen for each platelet was the longest chord within the particle. The morphological parameters of the three size fractions deduced from the analysis of around 100–150 particles are shown in Table 1 and their size distributions are plotted as histograms in Figure 1. Small amounts of kaolinite are still present in sizes 1 and 2, even after purification. The average diameters are 325, 285, and 210 nm for sizes 1–3, respectively. The histograms illustrate the polydispersity of clay systems with sizes ranging from 50 to 950 nm. The polydispersity still remains relatively high after size selection; this parameter slightly decreases from size 1 to size 3 with values of 47, 45, and 38%.

Osmotic Pressure Measurements. The osmotic pressure curves obtained for the three size fractions and at different ionic strengths are displayed in Figure 2.

Whatever the size or the ionic strength, all curves look similar. At low volume fraction, the osmotic pressure increases rapidly up to 1000 Pa followed by a more moderate increase. However, the so-called “pseudoplateau” observed for laponite¹⁹ and Wyoming montmorillonite²¹ is not really observed in the case of beidellite at ionic strengths lower than 10^{-3} M/L. Above 2500 Pa, the osmotic pressure increases quickly again. The influence of ionic strength is particularly visible at high concentration, where an increase in ionic strength reduces the osmotic pressure, in agreement with a decrease of the Debye length. For a given ionic strength, a decrease in particle size shifts the osmotic pressure toward higher values (Figure 2d) in agreement with an increase in the number of particles for identical volume fractions.

Optical Observations. Vials filled with aqueous beidellite suspensions at various volume fractions were examined at regular time intervals after preparation. Just after sample homogenization, gentle flow of the samples induces a transient birefringence, which decays slowly with time (flow birefringence). After three months, depending on volume fraction, a clear change of the optical properties of the samples is observed for both size 2 and size 3 (Figure 3) samples. In size 1 samples, platelet sedimentation takes place, which hampers the observations.

At low volume fractions, the samples are isotropic liquids (Figure 3a). Still, they exhibit flow birefringence (Figure 4) with relaxation times that increase with the volume fraction and can reach up to a few seconds. Such pretransitional effects, strongly suggest liquid-crystalline behavior at higher volume fractions.

Beyond a given volume fraction (Figure 3b), the samples are biphasic, with a birefringent nematic (N) bottom phase and an isotropic (I) upper one. These two fluid phases of almost equivalent volume fractions are separated by a sharp interface.

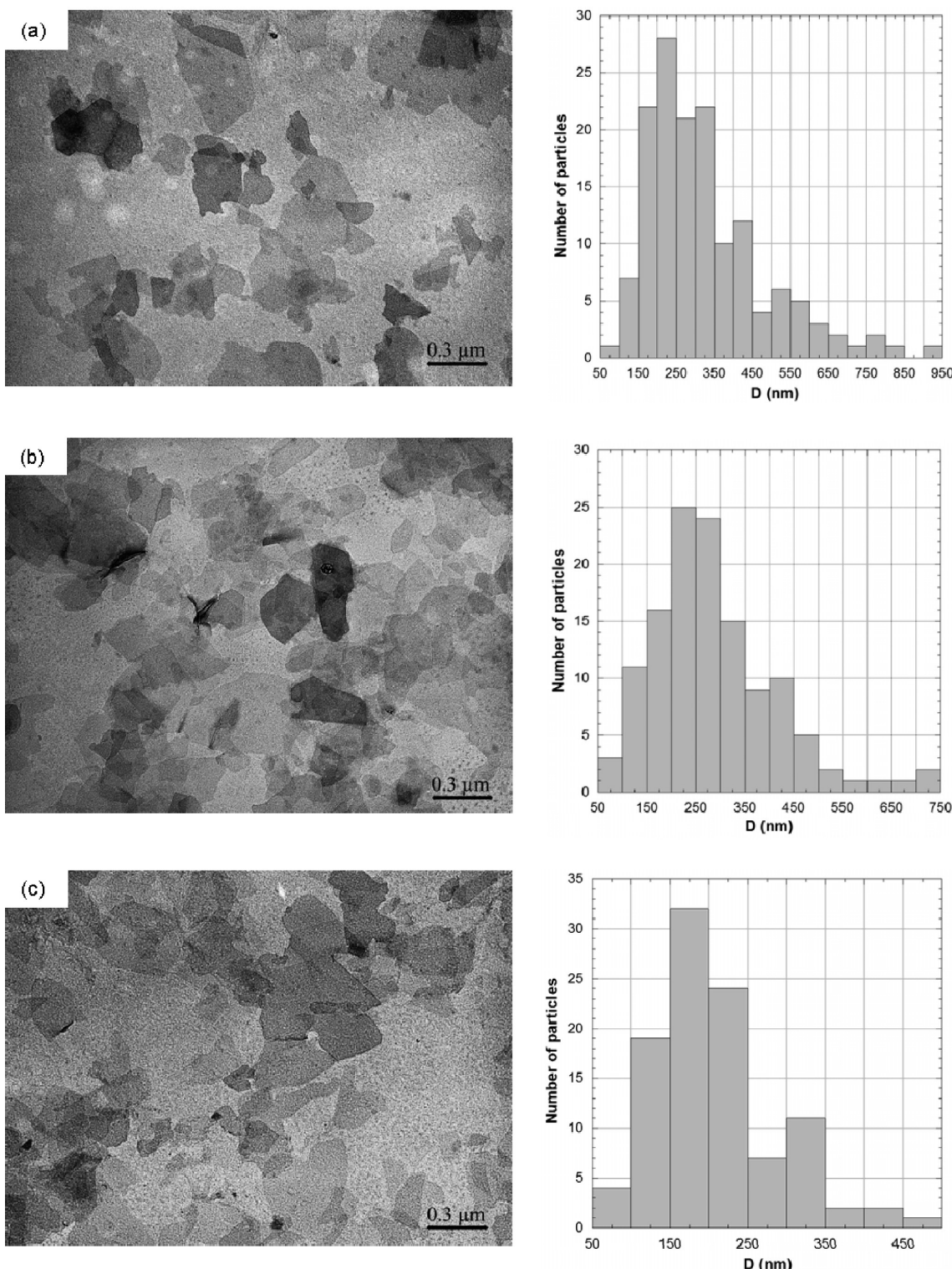


Figure 1. TEM micrographs and diameter distribution histograms of Na-SBId-1 subhedral platelets. (a) Size 1; (b) size 2; (c) size 3.

TABLE 1: Morphological Parameters of the Three Beidellite Size Fractions Obtained from the Analyses of TEM Micrographs

size	D_{\min} (nm)	D_{\max} (nm)	$\langle D \rangle$ (nm)	σ_D
1	94	900	326	47
2	77	729	286	45
3	69	480	209	38

The relative proportion of the nematic phase increases with total clay volume fraction. These features thus reveal a first order

isotropic/nematic transition and prove that the suspensions reach thermodynamic equilibrium. In contrast, at even higher volume fractions, no phase separation occurs and the suspensions form strongly birefringent gels. As mentioned above, for the largest size fraction sedimentation occurs and the I/N phase transition is not as clearly observed.

The I/N transition can also be followed by polarized light microscopy. A few days after sample preparation, in the biphasic region of the phase diagram birefringent nematic droplets (also called “tactoids”) appear and grow in the isotropic phase, then

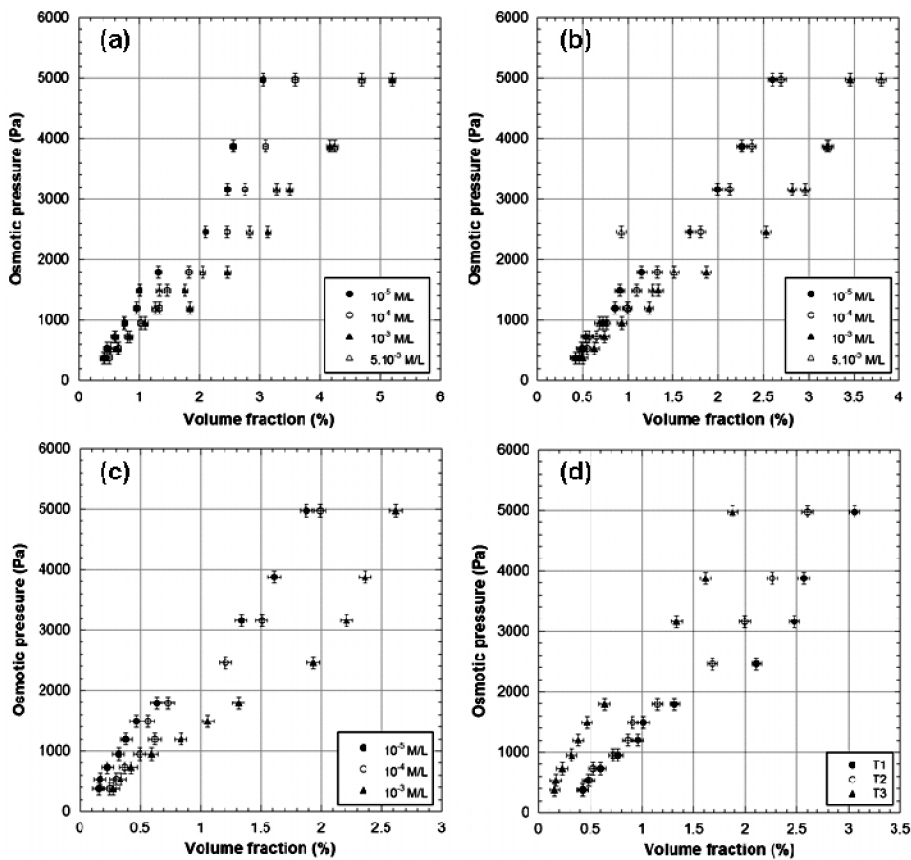


Figure 2. Osmotic pressure curves for the three size fractions of Na-SBId-1. (a) Size 1; (b) size 2; (c) size 3; (d) comparison of the three sizes at 10^{-5} M/L.

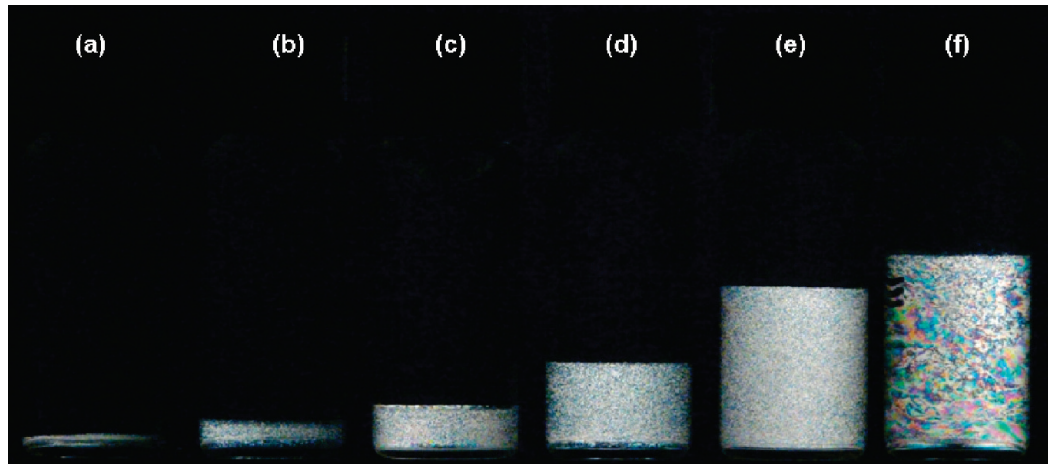


Figure 3. Aqueous suspensions of size 3 beidellite at an ionic strength of 10^{-4} M/L observed between crossed polarizer and analyzer. (a) $\phi = 0.40\%$; (b) $\phi = 0.42\%$; (c) $\phi = 0.44\%$; (d) $\phi = 0.46\%$; (e) $\phi = 0.48\%$; (f) $\phi = 0.50\%$.

sediment and coalesce to form a nematic phase at the bottom of the capillaries (Figure 5). The nematic phase displays the usual “threaded texture” of nematic phases.

As already mentioned, at higher volume fractions, the suspensions are brightly birefringent gels that display flow-alignment and threaded or Schlieren textures.

Rheological Measurements. The variation of the elastic modulus G' with oscillatory frequency for different volume fractions at an ionic strength of 10^{-4} M/L is presented in Figure 6. All size fraction of beidellite present similar evolutions. For suspensions of low volume fractions, the elastic G' and viscous G'' (not shown) moduli are of the same order of magnitude and exhibit a frequency dependence, corresponding to the behavior

of a slightly viscous liquid. For the higher volume fractions, G' is significantly larger than G'' and both moduli only exhibit a small frequency dependence, a feature typical of a gel. Furthermore, G' values exhibit some kinks in the high frequency region, which shift toward higher frequencies with increasing G' . Such variations can be attributed to inertial effects of the rheometer as demonstrated earlier.⁴⁶ Oscillatory measurements then provide a relatively quick way to determine the volume fraction of the sol/gel transition, even if modeling the flow curves was recently shown to be better suited for this purpose because of the slight elasticity of the liquid nematic phase that occurs before the gel state.^{34,35} Still, in the present paper, we use the results of oscillatory measurements to determine the

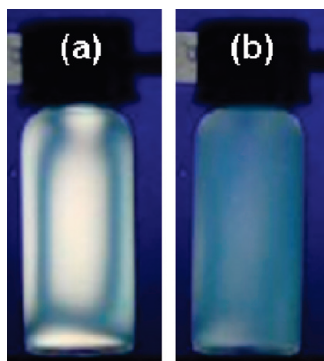


Figure 4. Aqueous suspension of size 2 beidellite (ionic strength: 10^{-3} M/L, $\phi = 0.43\%$) showing (a) flow birefringence (photograph taken right after flow) and (b) relaxation after the flow.

phase diagrams and a more detailed rheological analysis will be presented in a forthcoming paper. The viscoelastic behavior of the suspensions and the volume fraction of the sol/gel transition are strongly affected by particle size. A decrease of the average clay platelet diameter leads to gelation at lower volume fractions, a feature already observed for montmorillonite and nontronite clays.^{21,33–35}

Phase Diagrams. Using optical observations and rheological measurements, the (volume fraction/ionic strength) phase diagrams were established for the three size fractions of beidellite (Figure 7). Whatever the size, the phase diagrams present similar features. At high ionic strength, that is, above 10^{-3} M/L, the sol/gel transition line displays a negative slope, a behavior already observed in other natural clays (Montmorillonite^{21,23,47} Nontronites^{32,35}) or synthetic compounds such as laponite^{17,20} or takovites.⁴⁸ As the transition line appears to join the flocculation line at low volume fractions and high ionic strength, this negative slope may be assigned to the presence of microflocculation processes. At lower ionic strength, the sol–gel transition line displays a positive slope, which hints at the repulsive nature of the interactions between platelets in such conditions.

The two smallest size fractions exhibit an N/I biphasic domain whereas the turbidity of the size 1 suspensions, due to the presence small amounts of kaolinite as well as to sedimentation, hinders the observation of the phase transition. In our study, unfortunately, the average size has only a limited influence on the position of the transitions because of the small size difference between size 2 and 3 beidellite samples (Table 1). Moreover,

the exfoliation of size 2 beidellite is actually not quite complete and an appreciable proportion of particles composed of two clay sheets still remains (see the end of Section 3-2). This reduces the effective particle volume fraction, thus shifting the phase transition of size 2 beidellite suspensions toward larger concentrations. Besides, the positions of the isotropic and nematic binodals of the biphasic domain move only slightly toward lower volume fractions with decreasing ionic strength, even though it was varied over two decades. Moreover, the sol–gel transition line moves closer to the nematic domain and even crosses it at very low ionic strength ($\sim 10^{-5}$ M/L), leading to “freezing” of the suspension organization by the gelation process. A similar situation may also be present at higher ionic strength ($\sim 5 \cdot 10^{-3}$ M/L).

According to the phase diagrams, the positions of the isotropic and nematic binodals mainly depend on the size of the platelets since the influence of ionic strength remains rather limited. At this stage, the values of the I/N transition number densities obtained for the two smallest size fractions can be compared with theoretical ones. Computer simulations^{11,49} have established the dimensionless densities and pressure of the coexisting phases for the I/N transition of infinitely thin platelets, which are

$$n_I \langle D^3 \rangle \approx 3.7 \quad n_N \langle D^3 \rangle \approx 4 \quad (3)$$

where n_I and n_N represent the number densities in the isotropic and nematic phases, respectively, and D is the particle diameter. Assuming circular disk-shape morphology, the volume of size-selected beidellite particles is calculated as

$$v_{\text{disk}} = \frac{\pi}{4} \langle D^2 t \rangle \quad (4)$$

where t is the particle thickness. Thus, combining eqs 3 and 4, the dimensionless densities can be converted to theoretical isotropic and nematic volume fractions. By using information from Table 1 and the disk thickness (obtained for the two smallest sizes by X-ray scattering, see below), the I/N transition is predicted to occur at $\phi_I = 0.54$ and $\phi_N = 0.58\%$ for size 2 and at $\phi_I = 0.57$ and $\phi_N = 0.62\%$ for size 3. The agreement between calculated and experimental values is rather satisfactory considering that these theoretical simulations do not take into account the observed ionic strength dependence or the polydispersity in size.

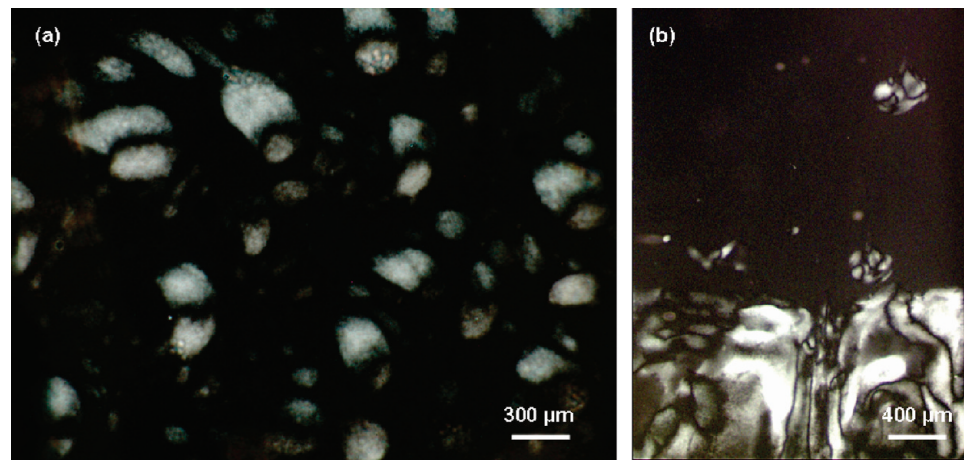


Figure 5. Formation of nematic droplets (tactoids) in aqueous suspensions of beidellite at 10^{-4} M/L, observed by polarized light microscopy. (a) Size 2, $\phi = 0.68\%$ (0.1 \times 1 mm flat capillary); (b) size 3, $\phi = 0.50\%$ (0.2 \times 2 mm flat capillary).

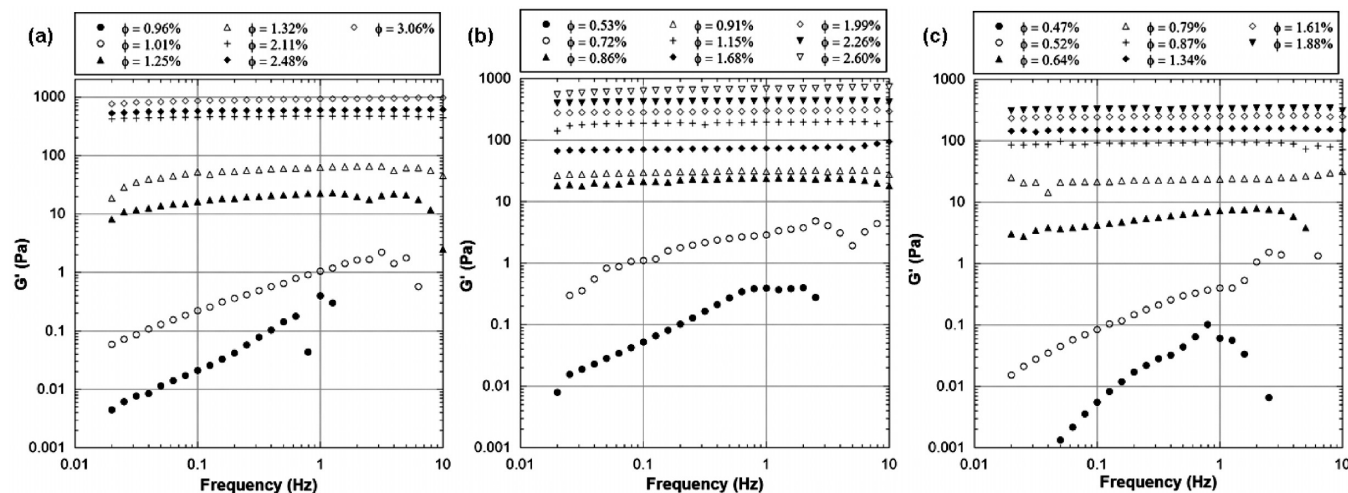


Figure 6. Variation of the elastic modulus G' with oscillatory frequency at an ionic strength of 10^{-5} M/L and different volume fractions. (a) Size 1; (b) size 2; (c) size 3.

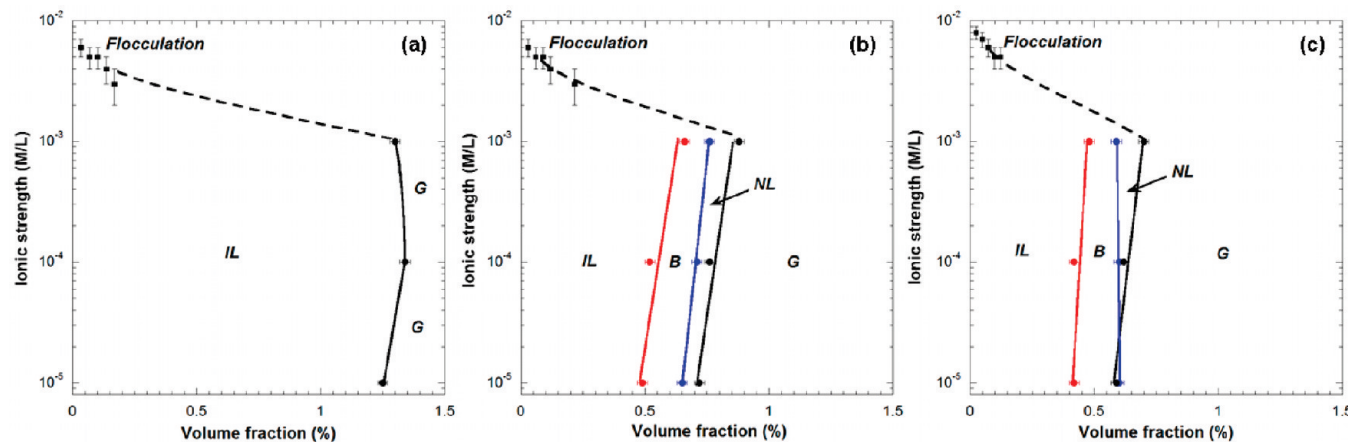


Figure 7. Phase diagrams obtained for the size-selected aqueous beidellite suspensions. (a) Size 1; (b) size 2; (c) size 3. IL = Isotropic liquid, B = Biphasic liquid, NL = Nematic Liquid, G = Gel.

As discussed in previous studies,^{33,35} upon increasing volume fraction, two other natural clays, namely nontronites NAu1 and NAu2, present a true isotropic to nematic phase transition before gelation occurs, in sharp contrast with montmorillonite and laponite. As the morphologies of nontronite and beidellite are different (lath-shaped for the former and disk-shaped for the latter), the existence of an I/N transition cannot be assigned to a particular shape of the particles. Interestingly, the three clay suspensions that were so far reported to exhibit an I/N transition happen to be those for which the structural charge arises from the tetrahedral layer, that is, close to the particle surface, whereas the clay suspensions that only present a sol/gel transition are those for which the charge is located within the octahedral layer, that is, “buried” in the structure. The location of structural charge could then somehow control the occurrence of an I/N transition. This may be related to subtle electrostatic effects such as changes in the ionic condensation at the disk surface. More simulation and experimental work is clearly needed before this issue can be fully solved.

2. Structural Characterization. To assess the structure of the suspensions, SAXS measurements have been performed throughout the whole phase diagrams of size 2 and size 3 beidellite aqueous suspensions. In the isotropic state, very dilute suspensions (Figure 8) present a monotonous decay of the scattered intensity I with scattering vector modulus q , that scales as $I(q) \sim q^{-2}$. Actually, this feature is the particle form factor

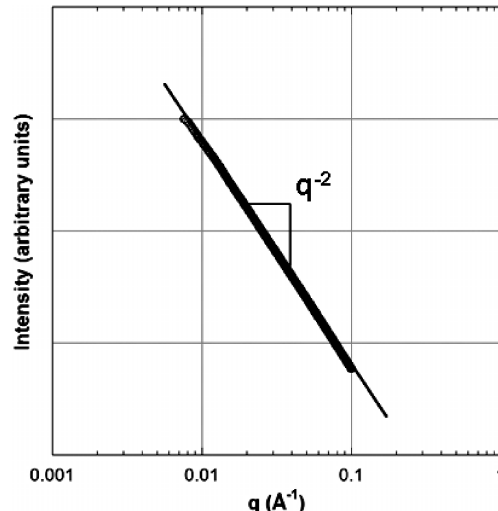


Figure 8. Variation of the scattered intensity as a function of q for a size 3 beidellite suspension in the dilute regime ($\phi = 0.43\%$, ionic strength = 10^{-3} M/L).

that describes the scattering by an isotropic distribution of noninteracting 2D objects, in the so-called “intermediate regime” where $2\pi/D < q < 2\pi/l$.

At higher volume fractions, just below the I/N transition line, the SAXS patterns are still isotropic (inset of Figure 9a) but

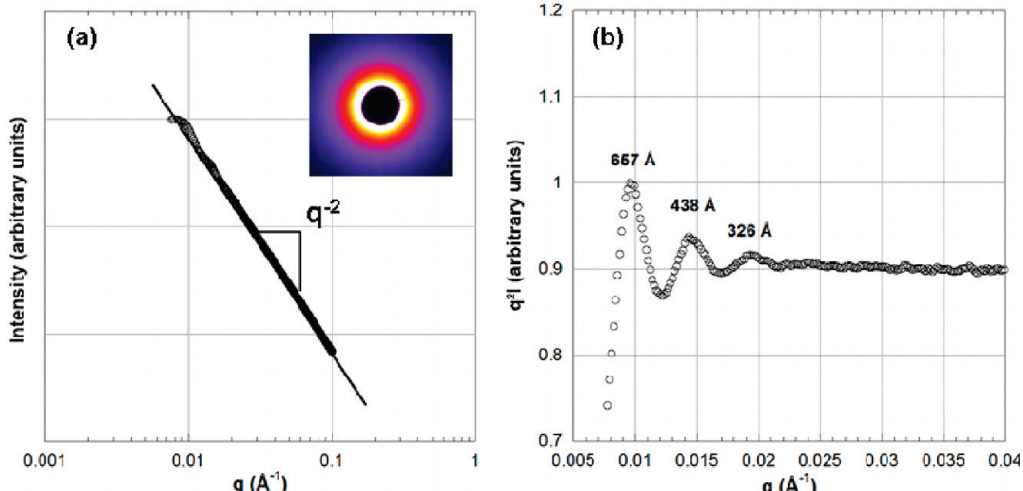


Figure 9. Variation of (a) the scattered intensity and (b) the structure factor $q^2 I(q)$ as a function of q of a size 3 beidellite suspension in the isotropic phase ($\phi = 0.39\%$, ionic strength = 10^{-5} M/L). The inset in (a) shows the 2D-SAXS pattern of the suspension. The first order in (b) that would correspond to a distance of about 1300 Å cannot be detected on this pattern.

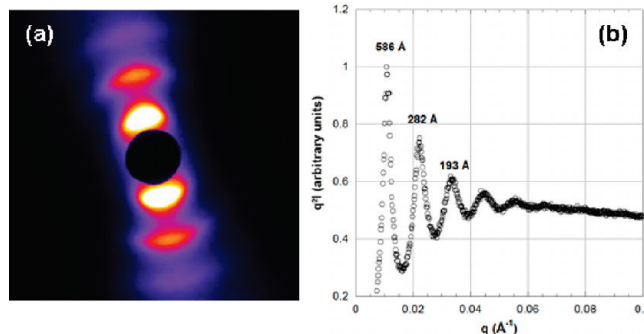


Figure 10. (a) 2D-SAXS pattern of the gel phase and (b) associated curves $q^2 I(q)$ of size 3 beidellite suspensions at an ionic strength of 10^{-4} M/L and $\phi = 1.21\%$.

display a periodic modulation of the scattered intensity due to short-range positional (i.e., “liquidlike”) order of the platelets (Figure 9b). The average interparticle distance, d , can be roughly estimated from the positions of the maxima of these oscillations $q_{\max}, 2 q_{\max}, 3 q_{\max}, \dots$ as $d \approx (2\pi)/(q_{\max})$.

In the biphasic domain, the two-dimensional patterns of the nematic phases are anisotropic because the samples are more or less aligned by the shear flow that takes place when the capillaries are filled with samples.³³

Finally, above the sol–gel transition, the patterns of gel samples exhibit a strong anisotropy because of the alignment due to capillary filling and display marked diffuse peaks located at higher q values, and thus corresponding to shorter interparticle distances (Figure 10).

As discussed before,^{33,35} the swelling laws, that is, the evolution of the average interparticle distance as a function of volume fraction, provides information on the local structure of the suspensions. The swelling laws of size 2 and size 3 beidellite suspensions are presented in Figure 11.

Similar swelling laws are observed for size 2 and size 3 beidellite suspensions. At high volume fractions in the gel phase, the interparticle distance scales as ϕ^{-1} , indicating a local lamellar order of the beidellite platelets. Such behavior has already been observed for other clays such as montmorillonite^{50,51} or nontronites.^{32,35} At lower volume fractions, this 1D swelling regime disappears and a crossover takes place probably toward

a $\phi^{-1/3}$ regime due to the 3D swelling of noninteracting objects. This latter regime is better observed in the case of nontronite clays.

Figure 11 shows that the ionic strength, although varied over two decades, has only a marginal influence on the swelling laws. In contrast, increasing size clearly shifts the swelling curves to higher volume fractions.

The 1D swelling regime, observed at high volume fractions, is actually that expected for the dilution of a lamellar phase. Even though the liquid-crystalline phase of these beidellite suspensions is nematic rather than lamellar (the structure factor in Figure 10B is closer to that of a 1D liquid and the phase diagram with a nematic bimodal is different from that of a lamellar phase,⁵² we can use this regime to derive the thickness, t , of the individual objects, from the slope of the swelling law

$$d = \frac{\langle t \rangle}{\varphi} \quad (5)$$

The average values obtained from size 2 and size 3 are 0.91 and 0.6 nm, respectively. The latter value is close to that of a single clay sheet (0.625 nm), proving the perfect exfoliation of the layers in size 3 suspensions whereas the thickness obtained for size 2 suggests that the delamination is actually not quite perfect. Two different particle populations, in about equal amounts, would coexist in size 2 beidellite suspensions, one of perfectly delaminated sheets and another of two-layer sheets.

3. Orientation of the Fluid Nematic Phase by External Fields. Magnetic-Field Alignment. In contrast with the case of nontronite,³² beidellite suspensions could not be aligned in weak magnetic fields (1 T), whatever the platelet size, the volume fraction or the ionic strength, which is probably related to the very low amount of structural iron in these samples. Still, the fluid nematic phase of beidellite suspensions could be aligned using higher magnetic fields (~8 T) in about 15 h. Indeed, optical microscopy observations (Figure 12) reveal that the threaded texture is replaced by a homogeneous planar texture arising from the fact that the clay platelets align their normal parallel to the magnetic field direction.

Using these single-domain nematic samples, the birefringence Δn of the suspensions could be determined. Δn is negative (i.e., $n_0 > n_c$), as can be expected from the shape of the particles. For

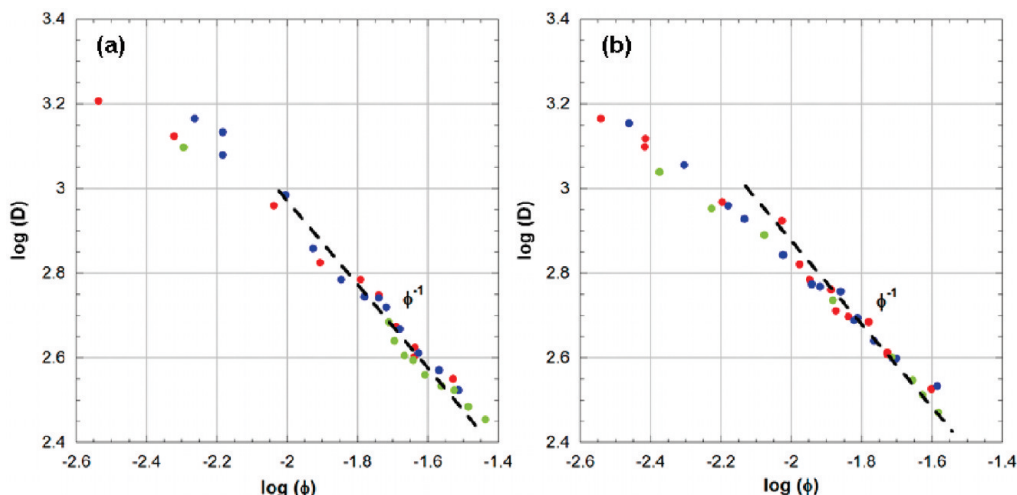


Figure 11. Variation of the average interparticle distance with volume fraction for different ionic strengths. (a) Size 2; (b) size 3. Ionic strength: red circles = 10^{-5} M/L, blue circles = 10^{-4} M/L, green circles = 10^{-3} M/L

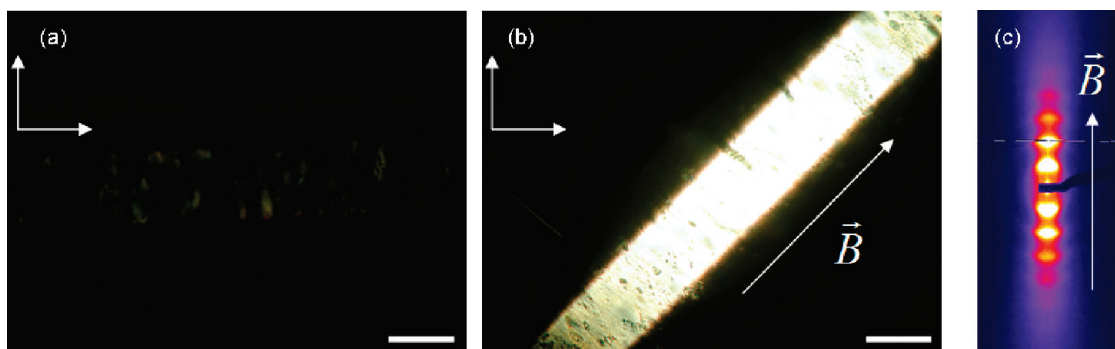


Figure 12. Optical textures in polarized light microscopy and SAXS pattern of a fluid nematic phase of size 3 beidellite suspension at an ionic strength of 10^{-4} M/L and $\phi = 0.62\%$ held in a 1 mm cylindrical glass capillary and submitted to a 8 T magnetic field during 15 h. Photographs were taken at (a) 0° , extinction, and (b) 45° , maximum of transmission. The crossed polarizer and analyzer are indicated by the white arrows whereas the scale bar represents 1 mm (c) SAXS pattern of size 3 beidellite suspension at an ionic strength of 10^{-4} M/L and $\phi = 0.52\%$ previously submitted to a vertical 8 T magnetic field.

example, the birefringence of a size 3, $\phi = 0.62\%$ (ionic strength 10^{-4} M/L), beidellite nematic suspension was measured, $\Delta n = -(4.1 \pm 0.3) \times 10^{-4}$. Naturally, the precise value of Δn depends on the volume fraction and also on the ionic strength to a lesser extent.

Figure 12c displays the SAXS pattern of the fluid nematic phase of a size 3 beidellite suspension aligned in a magnetic field. As expected, this pattern is very anisotropic, confirming the strong alignment of the particles with their normal parallel to the field. The anisotropy of magnetic susceptibility defined as $\Delta\chi_m = \chi_{\parallel} - \chi_{\perp}$ is then positive. In the limit of strong liquidlike order of the clay platelets (as suggested from the relative sharpness and number of diffuse peaks) and neglecting the effect of their finite diameter, a clay platelet in a given orientation in direct space gives rise to a scattering in exactly the same direction in reciprocal space. Therefore, the angular dependence of the scattered intensity, versus azimuthal angle, along a circle going through the diffuse scattering maximum, directly reflects the nematic orientational distribution function (Figure 13). The second moment of this distribution is the well-known nematic order parameter, P_2 , also referred to as S ,¹ a very important parameter of the nematic phase. The value obtained $S = 0.76 \pm 0.03$ is quite high, as expected for the strongly first-order I/N transition of these suspensions of disklike particles. Moreover, the higher even moments P_4 and P_6 can also be calculated (Table 2).

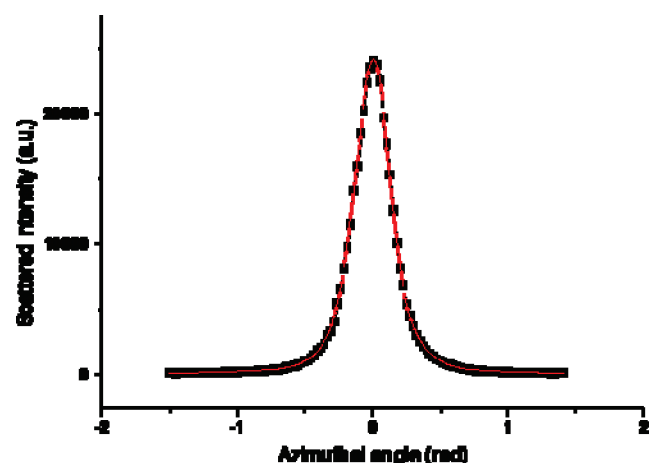


Figure 13. Orientational distribution function derived from the SAXS pattern (Figure 12c) of a beidellite suspension aligned in a magnetic field. The solid line is a fit used to calculate the moments of the distribution listed in Table 2.

Electric-Field Alignment. In contrast with the magnetic-field experiments, our electric-field setup allows us to perform in situ optical and SAXS experiments. Under moderate electric fields, the initially disoriented nematic texture in the capillary is progressively aligned (on the time scale of a few minutes up to a few hours, depending on the particles concentration) to give large and optically uniaxial domains.

TABLE 2: Values of the Nematic Order Parameter $S = P_2$, and the Higher Moments, P_4 and P_6 , of the Orientational Distribution Function, Obtained from the SAXS Patterns of the Samples Aligned by a Magnetic Field, an Electric Field, and by Homeotropic Anchoring^a

	$P_2 = S$	P_4	P_6
magnetic field	0.76	0.53	0.4
electric field	0.80	0.50	0.3
homeotropic	0.71	0.41	0.2

^a Error bars are estimated to ± 0.03 on P_2 , ± 0.05 on P_4 , and ± 0.1 on P_6 .

Figure 14 displays typical microscopic observations of the nematic texture of a beidellite suspension (size 3, ionic strength 10^{-4} M/L, $\phi = 0.62\%$) before (a,b) and after (c,d) the application of an electric field. The sample is contained in a flat optical capillary (0.2×2 mm cross section) and a 500 kHz ac field is applied for 10 min along the x -axis, parallel to the long axis of the capillary. Taking into account the corrections for the field penetration in the sample, we estimate the effective field to be $E = 7 \times 10^4$ V/m. The sample is observed along the z -direction between crossed polarizers, rotated together at 0 or 45° with respect to the x -axis. The initial texture is that of a typical randomly aligned and optically uniaxial nematic sample. Both the zenithal (θ) and azimuthal (φ) orientations of the optical axis, parallel to the local nematic director \mathbf{n} (i.e., to the average direction of the normal of the clay disks), vary smoothly across the sample. Rotating the crossed polarizers, we identify homeotropic (\mathbf{n} parallel to z) regions h , remaining black upon arbitrary rotation of the polarizers. The transmitted intensity in the tilted ($\theta \neq 0$) and planar ($\theta \approx \pi/2$) regions varies upon polarizers rotation, vanishing only when the projection of the director onto the xy -plane (shown on the figure by red arrows) is parallel to one of the polarizers.

After applying the electric field, the uniform black field of view in (c) reveals the director reorientation corresponding to $\varphi = \pi/2$ everywhere in the sample. However, the photograph (d) shows that the sample is actually not a single domain; the director tilt varies smoothly from $\theta = 0$ in the black homeotropic region h up to $\theta \approx \pi/2$ in the brightest planar region p . The nematic director is then perpendicular to \mathbf{E} , but its orientation is degenerated in the xz -plane. At longer times, the texture relaxes slowly to approximately uniform alignment, minimizing the distortion energy related to the director spatial variation.

The perpendicular orientation of the nematic director \mathbf{n} under electric field reveals that the dielectric anisotropy $\Delta\epsilon = \epsilon_{\parallel} - \epsilon_{\perp}$ of the beidellite suspension is negative. In other words, the platelets align their normal perpendicular to the field. The electric-field contribution to the free energy $-(1/2)\epsilon_0\Delta\epsilon(\mathbf{E} \cdot \mathbf{n})^2$ aligns the director \mathbf{n} in the plane perpendicular to \mathbf{E} , without imposing any particular direction of \mathbf{n} in this plane. The resulting degeneracy of the texture, as evidenced by Figure 14d, makes the accurate measurement of the birefringence more difficult, due to the unknown local tilt of the director in the studied area. The best estimate $\Delta n = -(4.7 \pm 0.4) \times 10^{-4}$, obtained from the maximal value of the measured local phase shift in the size 3, (ionic strength 10^{-4} M/L) $\phi = 0.62\%$ beidellite suspension, is in reasonable agreement with the value $\Delta n = -(4.1 \pm 0.3) \times 10^{-4}$ measured in a magnetic-field aligned domain in the same sample (see previous subsection).

The alignment of the nematic phase under electric field is confirmed by SAXS measurements (Figure 15c). For this purpose, the sample was prepared in a 1 mm cylindrical capillary and the electric field was applied in situ during the experiment. The quality of the field-induced alignment was controlled by polarized-light microscopy (Figure 15a,b) in a preliminary experiment. The SAXS pattern confirms the approximately uniform alignment of the sample with \mathbf{n} perpendicular to the field and the large value of the nematic order parameter (Table 2), in good agreement with the measurements with samples oriented in a magnetic field.

Homeotropic Alignment. When a sample of the fluid nematic phase of beidellite suspension is introduced in a flat capillary, it actually consists of many domains of different orientations separated by topological defects such as wall defects and disclination lines.¹ Indeed, examined by polarized light microscopy, samples freshly prepared in flat capillaries display the usual threaded texture of nematics with sometimes some global anisotropy of the texture, detected by SAXS, due to the flow that takes place when the capillary is filled. However, this threaded texture slowly evolves over a few weeks and becomes quite dark between crossed polarisers (Figure 16a). The clay platelets tend to align parallel to the flat walls of the glass capillary and this orientation, called “homeotropic anchoring”, propagates throughout the whole volume of the sample. At the end of this process, all topological defects have vanished and the sample is a nematic single domain with the director aligned perpendicular to the capillary flat walls. It should be noted that

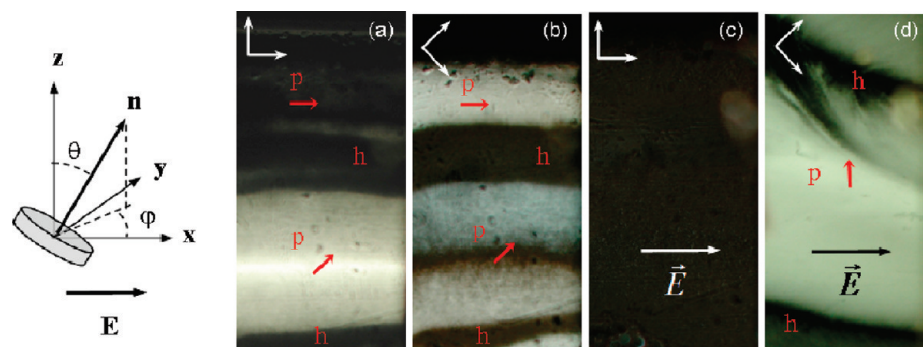


Figure 14. Optical analysis of the nematic texture of a beidellite suspension (size 3, ionic strength 10^{-4} M/L, $\phi = 0.62\%$) between crossed polarizers (shown as white arrows on the pictures) before (a,b) and after (c,d) the application of an electric field $E = 7 \times 10^4$ V/m. In the initial texture, both the zenithal (θ) and azimuthal (φ) orientations of the director \mathbf{n} vary across the sample. The regions h , remaining black upon arbitrary rotation of the polarizers, are homeotropic, with $\mathbf{n} \parallel z$. The regions p are almost planar, with $\theta \approx \pi/2$, and the red arrows show the projection of the director onto the xy -plane. The uniform black field in (c) reveals the director reorientation under the influence of the electric field with $\varphi = \pi/2$ everywhere. However, the photograph (d) shows that the sample is actually not a single domain; the director tilt θ varies smoothly from $\theta = 0$ in the black homeotropic region h up to $\theta \approx \pi/2$ in the brightest planar region p .

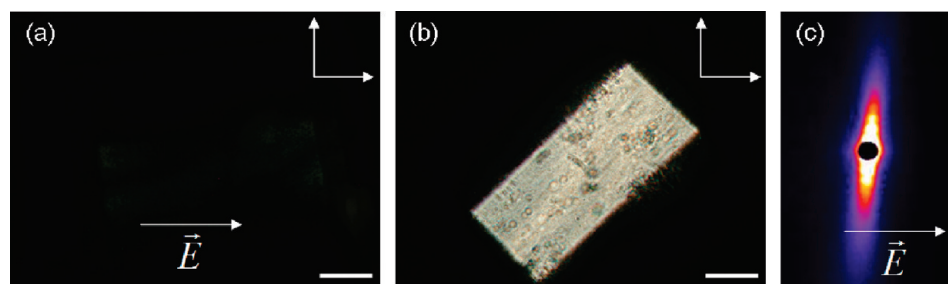


Figure 15. Optical textures in polarized light microscopy and SAXS pattern of fluid nematic samples of beidellite suspensions (a) size 2 (ionic strength = 10^{-5} M/L and $\phi = 0.61\%$) beidellite sample in a 1 mm cylindrical glass capillary aligned in a 4×10^4 V/m, 500 kHz electric field at (a) 0° , extinction; and (b) 45° , maximum of transmission. The crossed polarizer and analyzer are indicated by the white arrows whereas the scale bar amount to 500 μ m. (c) SAXS pattern of size 3 beidellite suspension (ionic strength = 10^{-4} M/L; $\phi = 0.52\%$) in a 1 mm cylindrical glass capillary aligned in a 4×10^4 V/m, 700 kHz horizontal electric field.

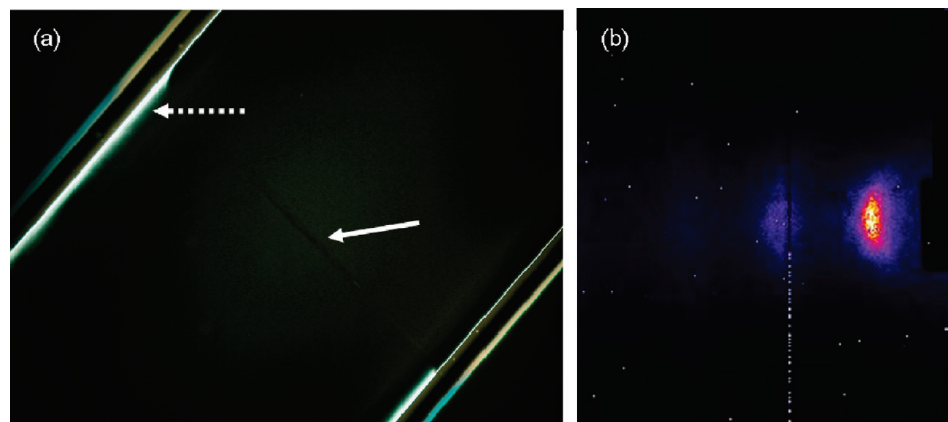


Figure 16. (a) Polarized light microscopy image of a biphasic sample of a beidellite suspension (size 3, ionic strength 10^{-4} M/L, $\phi = 0.57\%$) in a flat glass capillary (2 mm wide). The white arrow points to the (barely visible) meniscus between the isotropic phase in the upper right part and the nematic phase in the bottom left part. The nematic phase is in the homeotropic orientation due to wall-anchoring and therefore also appears as dark as the isotropic phase (nematic symmetry axis parallel to the light beam). The broken white arrow points to a bright area at the edge of the nematic phase where the anchoring is planar due to the influence of the side walls of the capillary. (b) SAXS pattern of a homeotropic nematic sample of size 3 beidellite suspension (ionic strength = 10^{-4} M/L; $\phi = 0.62\%$).

the nematic phase of gibbsite platelet suspensions (another “mineral liquid crystal”) also displays spontaneous homeotropic anchoring in flat glass capillaries.⁵³

In this geometry, the nematic director (the average orientation of the normals of the clay disks) is parallel to the microscope light beam and the sample does not appear birefringent because of the uniaxial symmetry of the nematic phase. Nevertheless, a SAXS experiment on the same sample, performed by shining X-rays in a direction perpendicular to the director reveals the strong anisotropy of the phase (Figure 16b).

Conclusion and Perspectives

Aqueous suspensions of size-selected natural beidellite clay display all the typical features of lyotropic nematic liquid crystals. In particular, the spontaneous homeotropic alignment of the samples fully proves the thermodynamic nature of the nematic ordering of these suspensions. Furthermore, the use of electric fields or magnetic fields and the spontaneous alignment provides several ways of obtaining nematic single domains of well-defined texture and anchoring. Such features are a prerequisite for performing more sophisticated experiments and to fully analyze the liquid crystal behavior of these suspensions. In addition, this could provide new ways for developing “smart” clay-based materials^{54,55} by taking full advantage of the orientation properties. For example, one may envision the synthesis of fully oriented clay–polymer nanocomposites with improved properties.

Moreover, some crucial points still remain unclear, in particular the influence of the charge location in the clay structure. As demonstrated, tetrahedrally substituted clays like nontronites and now, beidellite, show a true isotropic to nematic phase transition whereas all investigations carried on montmorillonite or laponite with an octahedral charge deficit lead to a recurrent sol/gel transition. Since the influence of particle shape seems to be limited in this respect, the electrostatic interactions mediated by ionic condensation at surfaces might play a crucial but subtle role. For instance, charge location might alter the network of water hydrogen bonds close to the clay surface, which may affect the surface hydrophilicity. This assumption is presently being investigated in our laboratory.

Acknowledgment. Authors gratefully acknowledge the SOLEIL synchrotron for awarding beamtime as well as financial support from the ANR (Agence Nationale de la Recherche, “programme blanc” ANISO). We would like to thank Sabine Manet for her help during SAXS experiments on beamline D2AM and Sandrine Mariot for help with the electro-optical measurements. We would also like to thank Jaafar Ghanbaja for his help in obtaining TEM micrographs.

References and Notes

- (1) De Gennes, P. G. *The Physics of Liquid Crystals*; Clarendon Press: Oxford, 1979.
- (2) Zocher, H. Z. *Anorg. Allg. Chem.* **1925**, *147*, 91–110.
- (3) Onsager, L. *Ann. N.Y. Acad. Sci.* **1949**, *51*, 627–659.

- (4) Davidson, P.; Batail, P.; Gabriel, J. C. P.; Livage, J.; Sanchez, C.; Bourgaux, C. *Prog. Polym. Sci.* **1997**, *22*, 913–936.
- (5) Sonin, S. A. *J. Mater. Chem.* **1998**, *8*, 2557–2574.
- (6) Gabriel, J. C. P.; Davidson, P. *Adv. Mater.* **2000**, *12*, 9–20.
- (7) Davidson, P.; Gabriel, J. C. P. *Curr. Opin. Colloid Interface Sci.* **2005**, *9*, 377–383.
- (8) Veerman, J. A. C.; Frenkel, D. *Phys. Rev. A* **1992**, *45*, 5632–5648.
- (9) Van der Kooij, F. M. *J. Phys. Chem. B* **1998**, *102*, 7829–7832.
- (10) Van der Kooij, F. M.; Kassapidou, K.; Lekkerkerker, H. N. W. *Nature* **2000**, *406*, 868–871.
- (11) Van der Kooij, F. M.; Van der Beek, D.; Lekkerkerker, H. N. W. *J. Phys. Chem. B* **2001**, *105*, 1696–1700.
- (12) Van der Beek, D.; Lekkerkerker, H. N. W. *Europhys. Lett.* **2003**, *61*, 702–707.
- (13) Wijnhoven, J. E. G. J.; Van't Zand, D. D.; Van der Beek, D.; Lekkerkerker, H. N. W. *Langmuir* **2005**, *21*, 10422–10427.
- (14) Brown, A. B. D.; Clarke, S. M.; Rennie, A. R. *Langmuir* **1998**, *14*, 3129–3132.
- (15) Brown, A. B. D.; Ferrero, C.; Narayanan, T.; Rennie, A. R. *Eur. Phys. J. B* **1999**, *11*, 481–489.
- (16) Langmuir, I. *J. Chem. Phys.* **1938**, *6*, 873–896.
- (17) Mourchid, A.; Delville, A.; Lambard, J.; Lécolier, E.; Levitz, P. *Langmuir* **1995**, *11*, 1942–1950.
- (18) Mourchid, A.; Delville, A.; Levitz, P. *Faraday Discuss.* **1995**, *101*, 275–285.
- (19) Mourchid, A.; Lécolier, E.; Van Damme, H.; Levitz, P. *Langmuir* **1998**, *14*, 4718–4723.
- (20) Mongondry, P.; Tassin, J. F.; Nicolai, T. *J. Colloid Interface Sci.* **2005**, *283*, 397–405.
- (21) Michot, L. J.; Bihannic, I.; Porsch, K.; Maddi, S.; Baravian, C.; Mougel, J.; Levitz, P. *Langmuir* **2004**, *20*, 10829–10837.
- (22) Emerson, W. W. *Nature* **1956**, *178*, 1248–1249.
- (23) Gabriel, J. C. P.; Sanchez, C.; Davidson, P. *J. Phys. Chem.* **1996**, *100*, 11139–11143.
- (24) Levitz, P.; Lécolier, E.; Mourchid, A.; Delville, A.; Lyonnard, S. *Europhys. Lett.* **2000**, *49*, 672–677.
- (25) Lemaire, B. J.; Panine, P.; Gabriel, J. C. P.; Davidson, P. *Europhys. Lett.* **2002**, *59*, 55–61.
- (26) Bhatia, S.; Barker, J.; Mourchid, A. *Langmuir* **2003**, *19*, 532–535.
- (27) Martin, C.; Pignon, F.; Magnin, A.; Meireles, M.; Lelièvre, V.; Lindner, P.; Cabane, B. *Langmuir* **2006**, *22*, 4065–4075.
- (28) DiMasi, E.; Fossum, J. O.; Gog, T.; Venkataraman, C. *Phys. Rev. E* **2001**, *64*, 061704.
- (29) Fonseca, D. M.; Meheust, Y.; Fossum, J. O.; Knudsen, K. D.; Parmar, K. P. S. *Phys. Rev. E* **2009**, *79*, 021402.
- (30) Pisey, C.; Klein, S.; Leach, E.; Van Duijneveldt, J. S.; Richardson, R. M. *J. Phys.: Condens. Matter* **2004**, *16*, 2479–2495.
- (31) Bihannic, I.; Michot, L. J.; Lartiges, B. S.; Vantelon, D.; Labille, J.; Thomas, F.; Susini, J.; Salomé, M.; Fayard, B. *Langmuir* **2001**, *17*, 4144–4147.
- (32) Michot, L. J.; Bihannic, I.; Maddi, S.; Funari, S. S.; Baravian, C.; Levitz, P.; Davidson, P. *Proc. Natl. Acad. Sci. U.S.A.* **2006**, *44*, 16101–16104.
- (33) Michot, L. J.; Bihannic, I.; Maddi, S.; Baravian, C.; Levitz, P.; Davidson, P. *Langmuir* **2008**, *24*, 3127–3139.
- (34) Michot, L. J.; Baravian, C.; Bihannic, I.; Maddi, S.; Moyne, C.; Duval, J. F. L.; Levitz, P.; Davidson, P. *Langmuir* **2009**, *25*, 127–139.
- (35) Michot, L. J.; Paineau, E.; Bihannic, I.; Maddi, S.; Duval, J. F. L.; Baravian, C.; Davidson, P.; Levitz, P. *Clay Miner.*, submitted for publication.
- (36) Gruner, J. W. *Am. Mineral.* **1935**, *7*, 475–483.
- (37) (a) Post, J. L.; Cupp, B. L.; Madsen, F. T. *Clays Clay Miner.* **1997**, *45*, 240–250. (b) Post, J. L.; Borer, L. *Appl. Clay Sci.* **2002**, *22*, 77–91.
- (38) Orsini, L.; Remy, J. C.; Henon, P. *Science du Sol* **1976**, *4*, 269–275.
- (39) Parsegian, V. A.; Rand, R. P.; Fuller, N. L.; Rau, D. C. *Methods Enzymol.* **1986**, *127*, 400–416.
- (40) Bonnet-Gonnet, C. Ph.D. Thesis, University of Paris VI, 1993.
- (41) Lécolier, E. Ph.D. Thesis, University of Orléans, 1998.
- (42) Michot, L. J.; Bihannic, I.; Pelletier, M.; Rinnert, E.; Robert, J. L. *Am. Mineral.* **2005**, *90*, 166–172.
- (43) Impérat-Clerc, M.; Davidson, P. *Eur. Phys. J. B* **1999**, *9*, 93–104.
- (44) Güven, N. In *Hydrous Phyllosilicates (exclusive of micas)*; Bailey, S. W., Ed.; Mineralogical Society of America: Washington, DC, 1988; Vol. 19, Chapter 13, pp 497–559.
- (45) Cadene, A.; Durand-Vidal, S.; Turq, P.; Brendle, J. *J. Colloid Interface Sci.* **2005**, *285*, 719–730.
- (46) Baravian, C.; Benbelkacem, G.; Caton, F. *Rheol. Acta* **2007**, *46*, 577–581.
- (47) Abend, S.; Lagaly, G. *Appl. Clay Sci.* **2000**, *16*, 201–227.
- (48) Michot, L. J.; Ghanbaja, J.; Tirtaatmadja, V.; Scales, P. J. *Langmuir* **2001**, *17*, 2100–2105.
- (49) Bates, M. A.; Frenkel, D. *J. Chem. Phys.* **1999**, *110*, 6553–6559.
- (50) Ramsay, J. D. F.; Swanton, S. W.; Bunce, J. *J. Chem. Soc., Faraday Trans.* **1990**, *86*, 3919–3926.
- (51) Ramsay, J. D. F.; Lindner, P. *J. Chem. Soc., Faraday Trans.* **1993**, *89*, 4207–4214.
- (52) Gabriel, J. C. P.; Camerel, F.; Lemaire, B. J.; Desvaux, H.; Davidson, P.; Batail, P. *Nature* **2001**, *413*, 504–508.
- (53) Van der Beek, D.; Davidson, P.; Wensink, H. H.; Vroege, G. J.; Lekkerkerker, H. N. W. *Phys. Rev E* **2008**, *77*, 031708.
- (54) Miyamoto, N.; Nakato, T. *Langmuir* **2003**, *19*, 8057–8064.
- (55) Nakato, T.; Yamada, Y.; Miyamoto, N. *J. Phys. Chem. B* **2009**, *113*, 1323–1331.

JP908326Y